Magnetic and dielectric properties of divalent Ca^{2+} and Ba^{2+} ions co-doped $BiFeO_3$ nanoparticles

N. Manjula, S. Ramu, K. Sunil Kumar, R.P. Vijayalakshmi*

Department of Physics, Sri Venkateswara University, Tirupati 517 502, India.

*Corresponding author

DOI: 10.5185/amlett.2018.1411
www.vbripress.com/aml

Abstract

Pristine $BiFeO_3$ (BFO) and Ca doped $BiFeO_3$: Ba nanoparticles (NPs) were synthesized in aqueous solution by sol-gel method with Tartaric Acid as a chelating agent. EDAX measurements confirmed the presence of Ca, Ba in the $BiFeO_3$ host lattice. X-ray diffraction analysis showed that the average grain size of the prepared samples was in the range of 09–28 nm. The lattice structure of the nanoparticles transformed from rhombohedral to tetragonal phase with Ca^{2+} ions substitution increased. TEM images indicated that sphere and square shape of nanoparticles through a size ranging from 10 to 15 nm. Diffusion reflectance spectra of $BiFeO_3$ NPs showed a substantial blue shift of ~100 nm (630 nm -> 530 nm) on Ca, Ba co-doping which corresponds to increase in band gap by 0.47 eV. Dielectric constant (ε') and dielectric loss (ε'') were measured in the frequency range 1 Hz to 1 MHz at room temperature. Dielectric constant and loss are increased with Ca concentration except for Ca (4 at. %). The bulk conductivity (σ) increases from 3.07 x 10^{-6} S/m to 1.64 x 10^{-5} S/m as the Ca concentration increased from 0.00 to 0.03. Magnetic measurements revealed the ferromagnetic character of Pristine BFO and Ca doped $BiFeO_3$: Ba samples. It is observed that by increasing the Ca concentration the value of M_r and magnetization are varied irregularly upto Ca (4 at. %). But for x = 0.01 M_r and magnetization are highest. The values of magnetization and M_r for 1% Ca doped $BiFeO_3$: Ba NPs are 2.99 emu/g, 1.54 emu/g, respectively, which are quite significant at room temperature. These materials have potential applications in data storage, switching devices, spintronics, sensors and microelectronic.

Keywords: Sol-Gel method, Ca doped $BiFeO_3$: Ba, band gap studies, magnetic properties, dielectric properties.

Introduction

In the present scenario a material with multiple properties is needed to meet the technological demand. The multiferroics possess multiple properties such as ferroelectric (Anti-ferroelectric), ferromagnetic (Anti-ferromagnetic) and ferroelasticity properties simultaneously. In view of this potential research is on multiferroics. They can be used in data storage, spintronics, sensors, quantum electromagnets and multistage memories [1-2]. One of the potential multiferroic material is $BiFeO_3$ (BFO) due to its high antiferromagnetic Neel temperature (T_N~640 K) and high ferroelectric Curie temperature (T_C~1100 K) [3] and also with small band gap. But BFO has some inherent problems, such as preparation of the phase pure compound, high leakage current, wide difference in ferroic transition temperatures and low magnetoelectric coupling coefficients. The problems can be rectified by suitable doping of rare earth (RE) ions (La, Pr, Nd, Gd, Ho etc.) at Bi-site [4–8] or substituting a part of Fe^{3+} ion by transition metal ions (Ti, Cr, Mn, etc.) [9–11].

Another possibility to enhance the magnetic and electric properties of BFO is by doping with divalent ions such as Ca^{2+}, Sr^{2+}, Ba^{2+} and Pb^{2+} at Bi site [12–13], which creates oxygen vacancies and transforms Fe^{3+} to Fe^{4+}, it will affect the degree of off-centering of FeO_6 octahedra and thus also dielectric and magnetic properties of BFO [13, 14–16]. B. Ramachandran et.al [17] reported weak ferromagnetic ordering at room temperature for Ba and Ba–Ca co-doped $BiFeO_3$ samples. Ba^{2+} doped $BiFeO_3$ prepared by chemical synthesis route showed the improvement of magnetoelectric coupling and maximum coupling reported for Ba doped $BiFeO_3$ is 20% [18].

The $BiFeO_3$ with different dopants were synthesized by the various research groups via sol-gel method [19] Priyanka Godara et al [20] reported Crystal structure transformation, dielectric and magnetic properties of Ba and Co modified $BiFeO_3$ multiferroic by sol-gel method. Ba and Co substitution transformed antiferromagnetic $BiFeO_3$ into ferromagnetic. Hernández et al [21] reported Characterization and magnetic properties of $Nd_xBi_{1-x}Fe_{0.95}Co_{0.05}O_3$ nano powders synthesized by combustion derived method at low temperature. NBFCO nanopowders displayed a ferromagnetic hysteresis loop, with coercivity about 0.1T and remanent magnetization of 1.02–4.33 Am^2/kg at room temperature. T. Durga Rao et al [22] synthesized Polycrystalline $BiFeO_3$ and rare earth substituted $Bi_{0.9}R_{0.1}FeO_3$ (BRFO, R=Y, Ho and Er) compounds by rapid solid state sintering technique and reported magnetic properties. S. Basu et al [23] have reported enhanced magnetic properties in hydrothermally synthesized Mn-doped $BiFeO_3$ nanoparticles by hydrothermal method.Recently, T. J. Park et.al [24] and

R. Mazumder et.al [25] reported room temperature ferromagnetism in $BiFeO_3$ nanoparticles. C.Yang et.al [14] have reported Magnetic and dielectric properties of alkaline earth Ca^{2+} and Ba^{2+} ions co-doped $BiFeO_3$ nanoparticles by a sol-gel method.

From the literature it is noticed that the defects and oxygen vacancies [26-27] influencing the multiferroic properties. In view of this present work is to investigate the effect of two different co-substituent cations Ca^{2+} (1.12 Å) and Ba^{2+} (1.42 Å) in which one is smaller in size to the parent cation and second is larger than parent cation Bi^{3+} (1.17 Å) on the structural, optical, magnetic and dielectric properties. The correlation between the structure and different properties is established based on the nature of two different co-substituents and their concentration.

Experimental

Sample Preparation

In the present work, $Bi_{0.95}Ba_{0.05-x}Ca_xFeO_3$ (x = 0.01, 0.02, 0.03 and 0.04) nanoparticles were prepared by sol-gel route. The reagents were of analytical grade and were used without further purification. Typical procedure followed is, Bismuth nitrate pentahydrate [$Bi(No_3)_3.5H_2O$], Iron nitrate nonahydrate [$Fe(No_3)_3.9H_2O$], Calcium nitrate tetrahydrate $Ca(NO_3)_2.4H_2O$ and Barium nitrate $Ba(NO_3)_2$ were weighed in stoichiometric proportions and dissolved in deionized water to make a solution with an independent concentration of 0.2 M, to this mixture 20 ml diluted nitric acid (65~68% HNO_3) was added and 10g of tartaric acid ((HOOCCH (OH) CH (OH) COOH)) was added to the solution as chelating agent. The light-yellow-colored transparent solution was heated under vigorous stirring in the oven at 160ºC for 4~5h. Subsequently, powders were calcined in the oven at 600ºC for 3h.

Characterization

Crystalline structure of the $Bi_{0.95}Ba_{0.05-x}Ca_xFeO_3$ particles were obtained using an X-ray diffractometer (model-3003TT) with Cu Kα radiation source (Wavelength, λ=1.5420 Å) in the 2θ range of 20^0-80^0 with a scan rate of 1º/min. The sample composition was obtained by Energy dispersive X-ray (EDAX) analysis. The particle size and structural studies has been carried out using transmission electron microscopy (TEM), and high-resolution TEM (HRTEM) of Hitachi-H7650. Ultraviolet-visible diffuse reflectance spectra (UV–Vis DRS) of the samples were measured by a JASCO V-670 UV-VIS-NIR Spectrometer. The magnetization of the BFO powders was carried out by using vibrating sample magnetometer (VSM) integrated in a physical property measurement system (PPMS-9, Quantum Design). Dielectric and conductivity studies were carried out using Impedance Analyzer (Model) solatron (SI 1260) General a.c circuit theory.

Results and discussion

Elemental analysis

In order to confirm the presence of Ba and Ca ions in the material, the EDAX spectra of co-doped samples were recorded. **Fig. 1 (a)-(e)** shows the EDAX spectra of $BiFeO_3$ and $Bi_{0.95}Ba_{0.05-x}Ca_xFeO_3$ (x = 0.01, 0.02, 0.03 and 0.04) nanoparticles respectively. From the spectra, it is obvious that the final product contains high atomic percentage of Bi and Fe as compared to the small doping concentrations of Ba and Ca ions. No traces of other elements were noticed in the spectra confirming the purity of the samples.

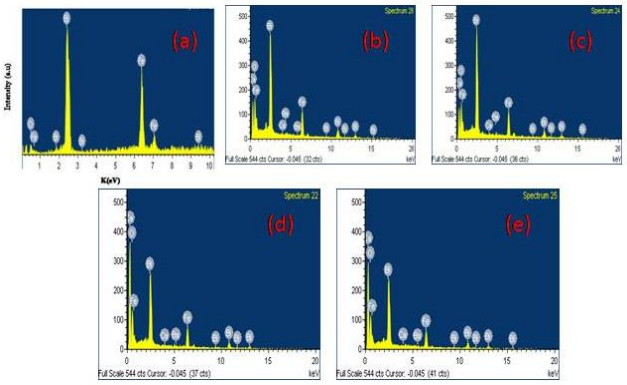

Fig. 1. (a)-(e) EDAX spectra of $BiFeO_3$ and $Bi_{0.95}Ba_{0.05-x}Ca_xFeO_3$ (x = 0.01, 0.02, 0.03 and 0.04) nanoparticles.

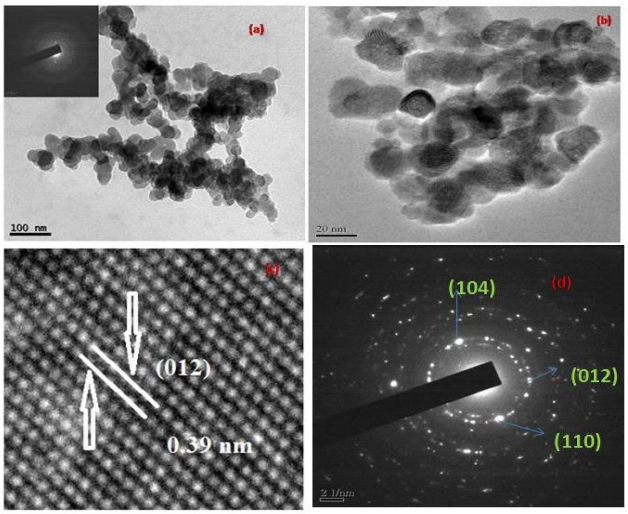

Fig. 2. (a) TEM image of BFO and inset SAED pattern **(b)** TEM image of Ca (1 at.%) doped $BiFeO_3$: Ba **(c)** HRTEM of Ca (1 at.%) doped $BiFeO_3$: Ba **(d)** SAED pattern of Ca (1 at.%) doped $BiFeO_3$: Ba Nanoparticles.

TEM analysis

To examine the microstructure of the present samples TEM analysis was carried out. **Fig. 2 (a)** shows the TEM image and SAED pattern (inset) of $BiFeO_3$ nanoparticles. It is evident from **Fig. 2 (b)** that spherical particle morphology of size around 25-30 nm for BFO and 10-15nm for Ca (1 at. %) doped $BiFeO_3$: Ba samples. **Fig. 2 (c) & (d)** shows the hi-resolution TEM (HRTEM)

image and typical SAED patterns for 1 at. % Ca co-doped $BiFeO_3$: Ba nanoparticles. The HRTEM picture clearly shows the lattice fringes. Distance between two adjacent planes is found to be 0.39 nm, which corresponds to a (012) plane of Ca (1 at %) doped $BiFeO_3$: Ba nanoparticles. The SAED pattern exhibits a concentric ring pattern from the (104), (110) and (021) diffraction planes.

Structural analysis

Fig. 3 (a) & (b) shows the XRD patterns of the un-doped BFO and Ca doped $BiFeO_3$: Ba nanoparticles at room temperature. The pure BFO is found to crystallize in rhombohedral structure with space group R3c with lattice parameters of a = b = 5.530A^o and c = 6.912A^o for pure BFO and lattice parameters of a = b = 5.571A^o and c = 13.646A^o for all co-doped samples. The average diameter of the particles was estimated using the Scherrer formula,

$$D = 0.89\ \lambda/\beta \cos\theta;$$

where D is the average size of the particles, β is the full width at half maximum intensity (FWHM) of the diffraction peak, λ is the wave length of X-rays used and θ is the angle of diffraction. The average size of the particles was found to be 28 nm for $BiFeO_3$ while for all the four co-doped samples it reduces to 9 nm. The substantial reduction of size in the co-doped samples may be due to restricted crystal growth as Ba^{2+} and Ca^{2+} ions are substitute in Bi^{3+} ion.

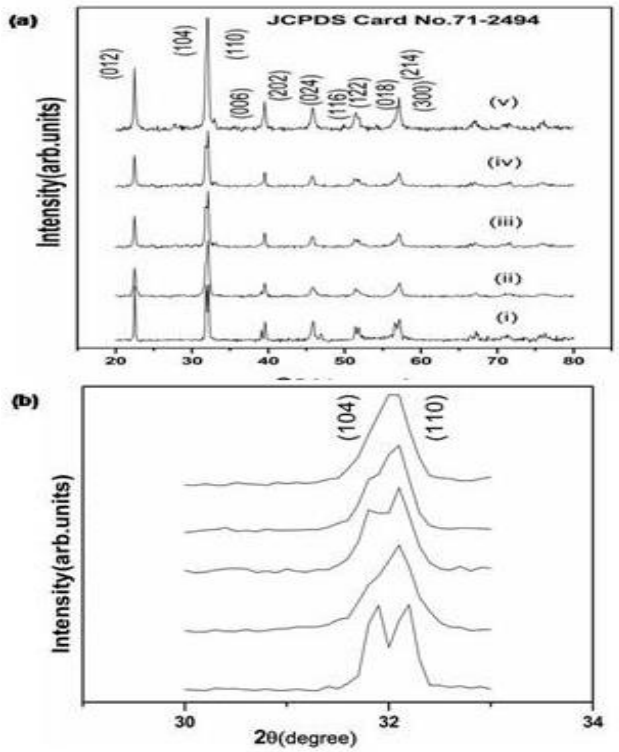

Fig. 3. (a) XRD patterns of (i) $BiFeO_3$ (ii) $Bi_{0.95}Ba_{0.04}Ca_{0.01}FeO_3$ (iii) $Bi_{0.95}Ba_{0.03}Ca_{0.02}FeO_3$ (iv) $Bi_{0.95}Ba_{0.02}Ca_{0.03}FeO_3$ (v) $Bi_{0.95}Ba_{0.01}Ca_{0.04}FeO_3$ **(b)** Shows the magnified patterns of (1 0 4) and (1 1 0) peaks around 32^o.

In pure $BiFeO_3$ the twin peaks were well separated such as (104) and (110), (006) and (202), (116), (122) and (018), (214) and (300). From Figure 3(b) it is noticed that these peaks (104) and (110) were merge into single peak for Ba 0.01 and Ca = 0.04. The merging of diffraction peaks clearly indicates the structural transformation from rhombohedral (R3c) to tetragonal structure. C.Yang et.al [14] reported that the lattice structure of the nanoparticles transformed from rhombohedral (x=0) to orthorhombic (x = 0.07–0.19) and to tetragonal (x = 0.20) with x increased for $Bi_{0.8}Ca_{0.2-x}Ba_xFeO_3$ (x = 0–0.20) samples.

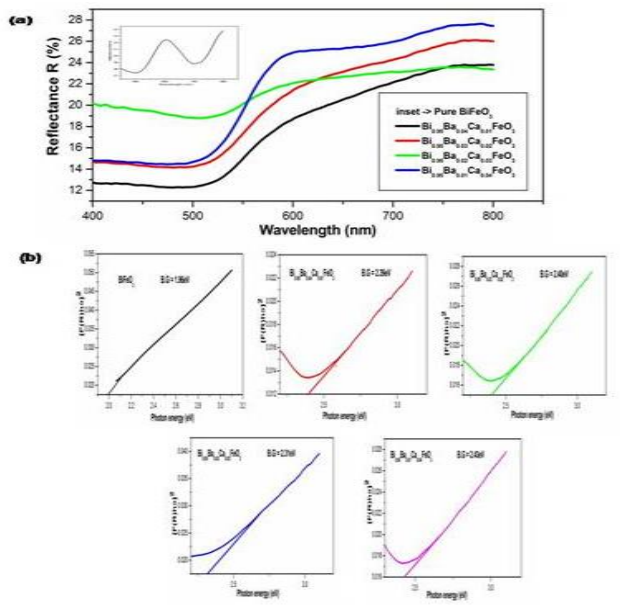

Fig. 4. (a) DRS spectra of Ca doped $BiFeO_3$: Ba nanoparticles and un-doped $BiFeO_3$ (inset) **(b)** Kubelka–Munk plots of Ca doped $BiFeO_3$: Ba nanoparticles.

Band gap studies

Reflectance measurements on un-doped $BiFeO_3$ and Ca doped $BiFeO_3$: Ba nanoparticles were done in the UV-visible region, 400-800 nm and the spectra are shown in **Fig. 4(a).** It is noticed that the absorption edge of the samples shifts slightly to lower wavelengths with increasing dopant concentration. As seen from the spectra, a significant shift of 100 nm towards the shorter wavelength is observed for Ca doped $BiFeO_3$: Ba nanoparticles. Pure $BiFeO_3$ nanoparticles exhibit absorption peak at 632 nm that shifts to 518, 516, 536 and 510 nm in the case of $Bi_{0.95}Ba_{0.04}Ca_{0.01}FeO_3$, $Bi_{0.95}Ba_{0.03}Ca_{0.02}FeO_3$, $Bi_{0.95}Ba_{0.02}Ca_{0.03}FeO_3$ and $Bi_{0.95}Ba_{0.01}Ca_{0.04}FeO_3$ respectively. The band gaps of the samples were estimated from diffuse reflectance spectra by plotting the square of the Kubelka-Munk function F (R) versus energy and extrapolating the linear part of the curve F $(R)^2$ =0 [28] as shown in **Fig. 4(b).** The band gap of $BiFeO_3$ NP is ~1.9 eV that widened to ~2.4eV in the case of co-doped samples and are shown in **Table 1**. In nanoparticles the common reason for this prominent blue shift could be the reduction of particle size of co-doped samples. But in the present study the size of Ca doped $BiFeO_3$: Ba nanoparticles is around 9 nm, which is larger

than quantum confinement region where particle size effect is dominant [29]. Hence, in the present work, the widening of the band gap is attributed to dopant ions. B. Bhushan et.al [30] reported an increase in band gap with Ca, Ba co-doped $BiFeO_3$ nanoparticles by sol-gel method. Vikash Singh et.al [31] reported a decrease in band gap in Pr and Ti co-doped nanoparticles by solid state reaction method. Prakash Chandra Sati et.al [32] reported a red shift in energy band gap with increasing concentration of Pr and Zr in $BiFeO_3$ ceramics by solid state reaction method.

Table 1. The band gap measurement of co-doped samples.

Sample	Band gap (eV)
$BiFeO_3$	1.96
$Bi_{0.95}Ba_{0.04}Ca_{0.01}FeO_3$	2.39
$Bi_{0.95}Ba_{0.03}Ca_{0.02}FeO_3$	2.40
$Bi_{0.95}Ba_{0.02}Ca_{0.03}FeO_3$	2.31
$Bi_{0.95}Ba_{0.01}Ca_{0.04}FeO_3$	2.43

Magnetization studies

Magnetization measurements at room temperature were carried out to understand the magnetic behavior of Ca doped $BiFeO_3$: Ba nanoparticles. Typical M-H curves of undoped $BiFeO_3$ and $Bi_{0.95}Ba_{0.05-x}Ca_xFeO_3$ (x = 0.01, 0.02, 0.03 and 0.04) nanoparticles are shown in **Fig. 5.** Magnetization curves are not saturated with the field up to 15 KG. From the **Fig. 5** it is clear that all samples exhibited hysteresis with magnetic field. Magnetic parameters associated with BFO and $BBCFO_x$ nanoparticles are summarized in **Table 2**. From **Table 2** it is observed that the value of H_c decreases with increasing x, but the value of M_r and magnetization are varying irregularly upto Ca (4 at. %). For x = 0.01 M_r, magnetization and H_c are highest. Ramachandran et al. [17] have reported weak ferromagnetic behavior in Ca (5 and 10 at. %) doped $BiFeO_3$ and they have not observed saturation magnetization even at applied field of 80 kOe. Sardar et al. [33] have observed weak ferromagnetic behavior with dopant concentration of 0.1 for Ca doped $BiFeO_3$ nanoparticles. Kothari et al. [34] have also observed weak ferromagnetic behavior in Ca-doped BFO thin films. S.F. Mansour et al. [35] also reported superparamagnetic behavior for Ca doped $BiFeO_3$ nanoparticles by the flash auto combustion technique. Rajasree Das et al [18] observed weak ferromagnetism behavior at 80 and 300 K for $Gd_{0.05}BFO$ and $Ba_{0.05}Gd_{0.05}BFO$ samples.

Table 2. Derived room-temperature magnetic parameters of BBCFOx.

Sample	Grain Size (nm)	H_c (Gauss)	M_r ($emug^{-1}$)	M $emug^{-1}$
$BiFeO_3$	27	124.2	0.64	2.90
$Bi_{0.95}Ba_{0.04}Ca_{0.01}FeO_3$	9	4828.3	1.54	2.99
$Bi_{0.95}Ba_{0.03}Ca_{0.02}FeO_3$	9	4090.9	0.67	1.35
$Bi_{0.95}Ba_{0.02}Ca_{0.03}FeO_3$	9	3956.9	1.44	2.82
$Bi_{0.95}Ba_{0.01}Ca_{0.04}FeO_3$	9	969.6	0.11	0.38

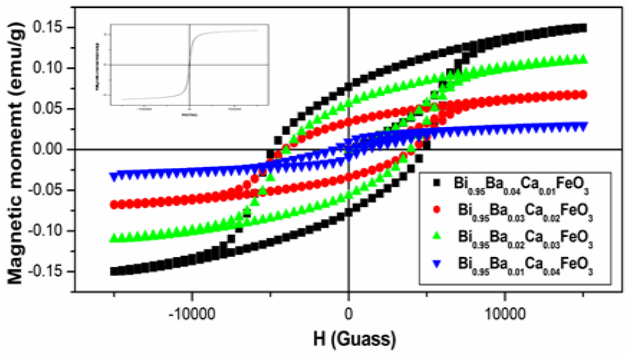

Fig. 5. Hysteresis loops of Ca doped $BiFeO_3$: Ba nanoparticles and un-doped $BiFeO_3$ (inset).

The enhanced magnetic properties of Ca doped $BiFeO_3$: Ba nanoparticles in comparison to the pure $BiFeO_3$ may be due to the existence of more uncompensated spins at the surface of co-doped $BiFeO_3$ nanoparticles because of their smaller size. Other possible reason for ferromagnetism in $BiFeO_3$ and Ca doped $BiFeO_3$: Ba nanoparticles is the modification of spiral spin structure characteristic of $BiFeO_3$ [29]. If the particle size is less than that of 62 nm, the spiral spin structure changes, leads to enhancement in magnetic properties. Substitution of Ba^{2+} and Ca^{2+} ions at Bi^{3+} site can cause a charge imbalance that can be compensated by conversion of Fe^{3+} ions to Fe^{4+} ions or by creation of oxygen deficiencies. So the only way to maintain the electro neutrality is the formation of oxygen deficiencies and these created oxygen deficiencies may be a possible reason for the enhancement in magnetic properties of the doped nanoparticles [36]. However, the nature of dopant and doping concentration playing pivotal role in determining the magnetic properties of $BiFeO_3$.

Dielectric properties

Dielectric analysis

Fig. 6 (a) & (b) illustrates the frequency (f) dependence of dielectric constant (ε') and dielectric loss (ε''), for BFO and $Bi_{0.95}Ba_{0.05-x}Ca_xFeO_3$ (x = 0.01, 0.02, 0.03 and 0.04) nanoparticles. For all the samples the dielectric constant (ε') and loss (ε'') are maximum at lower frequencies which decrease sharply with increasing frequency up to about 1 MHz and then become almost constant at high frequencies. At lower frequencies the higher dielectric constant may be due to the presence of electronic, ionic, dipolar and space charge polarizations whereas the lower value of dielectric constant at high frequency is due to electronic polarization. This is because larger size and mass of dipoles can respond only to low frequencies but at high frequencies they are unable to be in step with the frequency of the applied electric field and relaxed down [37]. This behavior is common in dielectric and ferroelectric materials [38]. The dielectric constant (ε') and dielectric loss (ε'') are not changing monotonically with Ca concentration. However the observed values of ε' and ε'' are lower for Ca 4% $BiFeO_3$: Ba than the BFO. This results shows that for 4% Ca concentrations

dielectric constant and loss are minimum. The possible reason for decrease dielectric constant and loss is due to decrease of oxygen vacancies. It is in concurrent with magnetic studies, for 4% Ca we observed low magnetization. The pellet for Ca (4 at. %) shows the lowest dielectric constant for all frequency range (1 Hz- 1 MHz) and the same pellet showed the lowest loss also for frequencies f<20 Hz. The loss is less in the present pellets may possibly assign to the low leakage current due to nano size grains. When the grain size in the pellets is small, the large insulating boundaries between the grains act as barriers for low leakage current. The crystalline structure and substitutional ions of the samples are the dominant factors affecting the dielectric properties of Ca doped $BiFeO_3$: Ba nano particles. Further, thorough investigations are needed to realize the detailed impacts of the properties of the crystalline structure and substitutional ions of the samples on the dielectric properties of Ca doped $BiFeO_3$: Ba samples. Pawan Kumar et al [39] reported the improved dielectric properties with very low value of dielectric loss for the $Bi_{0.95}La_{0.05}Fe_{0.95}Mn_{0.05}O_3$ synthesized by the tartaric acid modified sol-gel technique. Chou Yang et al [40] also reported decrease and increase of dielectric constants with increasing frequency in $Bi_{0.9-x}La_{0.1}Ca_xFeO_3$ (BLCFOx) (x = 0, 0.10, 0.13, 0.170.20) nano particles synthesized by sol-gel method.

Electrical analysis

The response of the real components of impedance (Z') with frequency at room temperature for BFO and $Bi_{0.95}Ba_{0.05-x}Ca_xFeO_3$ (x = 0.01, 0.02, 0.03 and 0.04) nanoparticles is shown in **Fig 6 (c)**. At higher frequencies > 10^5 Hz, Z' is almost independent of frequency, which is attributed to the resistance effect. In the frequency range (1Hz-1MHz), First Z' considerably decreases for all samples except for x = 0.04 with increasing frequency. This indicates that the components of capacity and resistance of the equivalent circuit are active in this sample in the range 1Hz-1MHz of frequencies. However, with frequency Z' decreases as Ca content increases till x = 3% and then Z' increases for Ca (at.4%), implying a decrease in the total resistance of the sample.

Fig. 6 (d) shows the variation of imaginary component of impedance (Z") with frequency at RT for BFO and $Bi_{0.95}Ba_{0.05-x}Ca_xFeO_3$ (x = 0.01, 0.02, 0.03 and 0.04) nanoparticles. The relaxation or Debye-type peaks in the low frequency region and the peak intensity is found to decrease at 3% and finally increases [41]. The increase in the imaginary component of the impedance (Z") indicates decrease of total resistance of the sample whereas the shift indicates increasing of relaxation time (tow) and loss in the material.

Fig. 6 (e) represents the Complex Impedance Cole–Cole [42] (imaginary part of the complex impedance: Z'' vs. real part of the complex impedance: Z') plot for BFO and $Bi_{0.95}Ba_{0.05-x}Ca_xFeO_3$ (x = 0.01, 0.02, 0.03 and 0.04) nanoparticles at room temperature in the frequency range of 1Hz – 1MHz. These plots are useful to get the

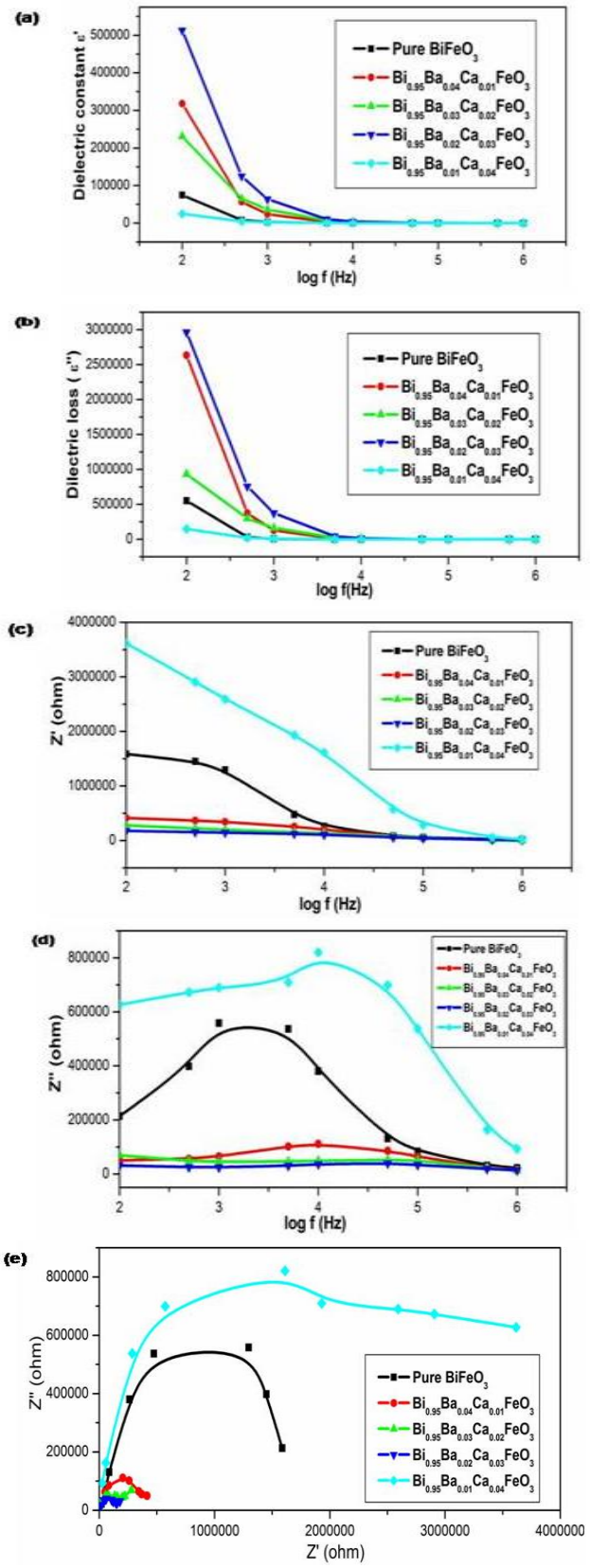

Fig. 6. Frequency dependence of **(a)** The dielectric constant and **(b)** Loss for BBCFOx nanoparticles **(c)** Real part of impedance with respect to frequency for different concentrations of Ba and Ca co- doped $BiFeO_3$ **(d)** Imaginary part of impedance with respect to frequency for different concentrations of Ba and Ca co-doped $BiFeO_3$ **(e)** Cole-Cole plots of Ba and Ca co-doped BiFeO.

information of scattering mechanisms with different relaxation times. From the figure it was evident that the radii of semicircle pattern decreasing with increasing Ca content till 3% , which indicates decrease in the total resistance of the sample and this explains the decrease of Z' and Z" as shown in **Fig 6 (c)** and **(d).** These graphs suggest that the grain and grain boundary contributions play a key role in the conduction mechanism for Ca doped $BiFeO_3$: Ba nanoparticles. More clearly, the semicircle in high frequency region is assigned to the grain property of the system, which originated from the parallel combination of grain resistance (R_g) and grain capacitance (C_g) of the system. Similarly, the semicircle in low frequency region is assigned to the grain boundary properties originated from the parallel combination of grain boundary resistance (R_{gb}) and grain boundary capacitance (C_{gb}) of the system. The possible factors that are responsible for the occurrence of the broad peak as a single semicircle in the nyquist plot of the Ca doped $BiFeO_3$: Ba sample may be due to the equal contributions from the grains and the grain boundaries with the applied external field. This could perhaps be due to the resistances offered by the grains and the grain boundaries may not be much different from one another as can be inferred from the corresponding fine grained microstructure.

The bulk conductivity (σ) value has been calculated using the formula [43],

$$(\sigma) = L/R_bA \ S\ m^{-1}$$

Where, R_b is bulk resistance of the sample
L is the thickness of the pellet
A is the effective area

The conductivity values are calculated from the above relation and it is observed that the conductivity increases from 3.07 x 10^{-6} S/m to 1.64 x 10^{-5} S/m as the Ca concentration increased from 0.00 to 0.03 and then the conductivity decreases from 3.07 x 10^{-6} S/m to 8.13 x 10^{-7} S/m from 0.00 to Ca (at. 4%). Similar results are reported on $BiFeO_3$ (BFO), Gd-doped $BiFe_{1-y}Gd_yO_3$ (y = 0.05, i.e. $Gd_{0.05}$BFO), Gd and Ba co-doped $Bi_{1-x}Ba_xFe_{1-y}Gd_yO_3$ (x, y < 0.1, i.e. $Ba_{0.05}Gd_{0.05}$BFO, $Ba_{0.05}Gd_{0.1}$BFO and $Ba_{0.1}Gd_{0.05}$BFO) samples prepared by a chemical synthesis route in ambient atmosphere [39].

Conclusions

In conclusion, Pure and $Bi_{0.95}Ba_{0.05-x}Ca_xFeO_3$ samples with x = 0.01, 0.02, 0.03 and 0.04 were synthesized by sol-gel method. The co-substitution of Ca and Ba has resulted in structural transition from rhombohedral perovskite structure to tetragonal structure as indicated by the XRD. EDS spectra confirmed the presence of Ca and Ba in the BFO lattice with expected stoichiometry. DRS spectra showed that as the Ca concentration increased the band gap shifted to higher energies indicating the improvement in crystallinity. TEM analysis revealed the creation of nanoparticles with average particle size in the range of 10-20 nm. Dielectric properties were measured upto frequency 1MHz. It was found that the co-doping of suitable amount of Ba^{2+} and Ca^{2+} ions was helpful to improve the dielectric properties of the samples. Ca doped $BiFeO_3$: Ba nanoparticles showed ferromagnetic hysteresis loop but decrease of ferromagnetism was observed with increasing the dopant Ca concentration. But the highest values of M_r and magnetization for Ca (1 at. %) doped $BiFeO_3$: Ba NPs are 1.54 emu/g and 2.99 emu/g. Co-doping has been found to be a better tool to tune the magnetic and dielectric properties. Magnetic and dielectric properties in a single material can be used in sensor and switching devices.

Acknowledgements

Authors would like to thank RGNF (Rajiv Gandhi National Fellowship), New Delhi for providing financial assistance.

References

1. Zavaliche, F.; Zhao, T.; Zheng, H.; Straub, F.; Cruz, M P.; Yang, P L.; Hao, D.; Ramesh, R; *nano lett*., **2007**, 7,1586. **DOI**: 10.1021/nl070465o
2. Spaldin, N A.; Feibig, M; *Science.*, **2005**, 309**,** 391. **DOI**: 10.1126/science.1113357
3. Prellier, W.; Singh, M.P.; Murugavel, P; *J. Phys.: Condens. Mater*., **2005**, 17, 803. **DOI**: http://iopscience.iop.org/0256-307X/10/1/017
4. Das, S.R.; Choudhary, R.N.P.; Bhattacharya, P.; Katiyar, R. S.; Dutta, P.; Manivannan, A.; Seehraet, M.S; *J. Appl. Phys.*, **2007**, 101, 034104. **DOI**: 10.1063/1.2432869
5. Khomchenko, V.A.; Troyanchuk, I.O.; Kovetskaya, M.I.; Kopcewicz, M.; Paixao, J.A; *J. Phys. D: Appl. Phys.*, **2012**, 45, 045302. **DOI**:10.1088/0022-3727/45/4/045302
6. Kumar, A.; Varshney, D; *Ceram. Inter.*, **2012**, 38, 3935; **DOI**:10.1016/j.ceramint.2012.01.046 Varshney. Dinesh.; Kumar A.; Verma K. J; *Alloys Compd.*, **2011**, 509, 8421. **DOI**: 10.1016/j.jallcom.2011.05.106
7. Lazenka, V.V.; Zhang, G.; Vanacken, J.; Makoed, I I.; Ravinski, A F.; Moshchalkov, V V; *J. Phys. D: Appl. Phys.*, **2012**, 45, 125002. **DOI**:10.1088/0022-3727/48/11/119501
8. Jeon, N.; Rout, D.; Kim, I.W.; et al., *Appl. Phys. Lett.*, **2011**, 98, 072901.
9. Qi, X.; Dho, J.; Tomov, R.; Blamire M.G.; Judith L.M.D; *Appl. Phys. Lett.* **2005**, 86, 062903. **DOI**: 10.1063/1.1862336
10. Chang, F.; Zhang, N.; Yang, F.;Wang S.; Song G; *J. Phys. D: Appl. Phys.*, **2007**, 40, 7799. **DOI:**10.1088/0022-3727/40/24/031
11. Kumar, M.; Yadav, K.L; *Appl. Phys. Lett.*, **2007**, 91, 242901. **DOI:** 10.1063/1.2816118
12. Khomchenko, V.A.; Kiselev, D.A.; Vieira, J.M.; Jian, L.; Kholkin, A.L.; Lopes, A.M.L.; Pogorelov, Y.G.; Araujo, J.P.; Maglione., M; *J. Appl. Phys.*, **2008**, 103, 024105. **DOI:** 10.1063/1.2836802
13. Bhushan, B.; Basumallick, A.; Bandopadhyay, S. K.; et al., *J. Phys. D*., **2009**, 42, 065004. **DOI:** 10.1088/0022-3727/42/6/065004
14. Yang , C.; Liu , C.Z.; Wang, C.M.; Zhang , W.G.; Jiang, J.S; *J. Mag, Mag. Mat.*, 2012, 324, 1483. **DOI:**10.1016/j.jmmm.2011.11.033
15. Zheng, W.; Yong, L.; Di, W.; et al., *Appl. Phys. Lett.*, **2011**, 99, 012903.
16. Lhomchenko, V.A.; Troyanchuk, I.O.; Karpinsky, D.V.; Paixao, J.A; *J. Mater. Sci.*, **2012**, 47, 1578. **DOI:** 10.1007/s10853-011-6040-4
17. Ramachandran, B.; Dixit, A.; Naik, R.; Lawes, G.; Ramachandra Rao M. S; *J. Appl. Phys.*, **2012**, 111, 023910. **DOI:**10.1063/1.3678449

18. Das, R.; Mandal, K; *J. Magn. Magn. Mater.*, **2012**, 324, 1913. **DOI:** 10.1016/j.jmmm.2012.01.022
19. Gurmeet Singh Lotey, Verma, N.K.; *Chem Phys Lett*., **2013**, 574, 71. **DOI**: 10.1016/j.cplett.2013.04.046
20. Priyanka Godara.; Ashish Agarwal.; Neetu Ahlawat.; Sujata Sanghi.; Reetu Dahiya.; *J. Alloys Compd*., **2014.** **DOI**: 10.1016/j.jallcom.2014.01.103
21. Hernández, N.; González-González, V.A.; Dzul-Bautista, I.B.; Cienfuegos-Pelaes, R.F.; Barandiaran, J.M.; Gutierréz, J.; Hernández, T.; Ortiz-Méndez, U.; Garcia-Loera, A.F; J. Magn. Magn. Mater., **2015**, 377, 466. **DOI**: 10.1016/j.jmmm.2014.10.158
22. Durga Rao, T.; Karthik, T.; Saket Asthana; *Journal of rare earths*., **2013**, 31, 370. **DOI**: 10.1016/S1002-0721(12)60288-9
23. Basu, S.; Hossain, SK. M.; Chakravorty, D.; Pal, M; *Curr.App.Phy*., **2011**, 11, 976. **DOI**: 10.1016/j.cap.2010.12.034
24. Park, T.J.; Papaefthymiou, G.C.; Viescas, A.J.; Moodenbaugh, A.R.; Wong, S.S.; *Nano Lett*., **2007**, 7 ,766. **DOI**: 10.1021/nl063039w CCC: $37.00
25. Mazumder, R.; Sujatha, D.P.; Bhattacharya, D.; Choudhury, P.; Sen, A.; Raja, M; *Appl.Phys.Lett*., **2007**, 91, 062510.
26. Guo, R.; Fang, L.; Dong, W.; Zhang, F.; Shen, M; *J. Phys. Chem. C*., **2010**, 114, 21390. **DOI:** 10.1021/jp 104660a
27. Madhu, C.; Bellakki, M.B.; Manivannan, V; *Indian J. Eng. Mat. Sci*., **2010**, 17, 131
28. Tauc, J.; Menth, A; *States in the gap. J. Non-Cryst. Solids*., **1972**, 8, 569. **DOI:** 10.1016/0022-3093(72)90194-9
29. Bhushan, B.; Wang, Z.; van Tol, J.; Naresh, S.D.; Basumallick A.; Vasanthacharya, N.Y.; Kumar, S.; Das, D; *J. Am. Ceram. Soc*., **2012**, 1–8. **DOI:** 10.1111/j.1551-2916.2012.05132.x
30. Bhushan, B.; Das, D.; Priyam, A.; Vasanthacharya , N.Y.; Kumar S; *Mater. Chem. Phys*., **2012**, 135, 144. **DOI:**10.1016/j.matchemphys.2012.04.037
31. Vikash Singh, Subhash Sharma, Manoj Kumar, Kotnala, R.K.; Dwivedi, R.K; *J. Mag, Mag. Mat*. **2014**, 349, 264. **DOI**: 10.1016/j.jmmm.2013.09.002
32. Prakash Chandra Sati, Manisha Arora, Sunil Chauhan, Sandeep Chhoker, Manoj Kumar; *J. Appl. Phys*., **2012**, 112, 094102. **DOI**: 10.1063/1.4761968
33. Sardar K.; Hong ,J.; Catalan ,G.; Biswas , P K.; Lees , M.R.; Walton, R.I.; Scott, J.F.; Redfern S.A.T; et al. *J. Phys.: Condens. Matter*., **2012**, 24**,** 045905. **DOI:** 10.1088/0953-8984/24/4/045905
34. Kothari, D.; Raghavendra Reddy, V.; Gupta, A.; Sathe, Vasant.; Banerjee, A; et al. *Appl. Phys. Lett*., **2007**, 91, 202505. **DOI:** 10.1063/1.2806199
35. Mansour S.F.; Abu-Elsaad, N.I.; Elmosalami, T.A; *Can.J.Phys*., **2014**, 92, 389. **DOI:** 10.1139/cjp-2012-0282
36. Sundaresan, A.; Bhargavi, R.; Rangarajan, N.; Siddesh, U.; Rao, C. N. R; *Phy. Rev*., 2006, 74, 161306. **DOI:** 10.1103/PhysRevB.74.161306
37. Uniyal, P.; Yadav, K.L; *Mater. Lett*., **2008**, 62**,** 2858. **DOI:** 10.1016/j.matlet.2008.01.103
38. Choudhary, R.N.P.; Pradhan, D.K.; Bonilla, G.E.; Katiyar, R.S; *ceramics, J. Alloys Compd*., **2007**, 437, 220. **DOI:** 10.1016/j.jallcom.2006.07.077
39. Pawan Kumar, Manoranjan Kar, *Mater. Chem. Phys*., **2014**, 148, 968. **DOI**: 10.1016/j.matchemphys.2014.09.007
40. Chou Yang, Ji-SenJiang, Chun-MeiWang, Wei-GuoZhang; *J. Phys. Chem. Solids*., **2012**, 73, 115. **DOI:** 10.1016/j.jpcs.2011.10.021
41. Chaudhuri, A.; Mandal K; *Mater. Res. Bull*., **2012**, 47, 1057. **DOI:** 10.1016/j.materresbull.2011.12.034
42. Wu, J.; Wang, J; *J. Appl. Phys*., **2009**, 105, 124107. **DOI:** 10.1063/1.3153955
43. Almond, DP; West, AR. *Solid State Ionics*., **1987**, 23, 27. **DOI:** 10.1016/0167- 38(87)900786.77–580.

